Pharm Res (2012) 29:2377–2388
DOI 10.1007/s11095-012-0763-z

RESEARCH PAPER

Influence of Molecular Size on the Retention of Polymeric Nanocarrier Diagnostic Agents in Breast Ducts

Yashveer Singh • Dayuan Gao • Zichao Gu • Shike Li • Kristia A. Rivera • Stanley Stein • Susan Love • Patrick J. Sinko

Received: 17 February 2012 / Accepted: 17 April 2012 / Published online: 9 May 2012

ABSTRACT

Purpose To investigate the influence of nanocarrier molecular size and shape on breast duct retention in normal rats using a non-invasive optical imaging method.

Methods Fluorescein-labeled PEG nanocarriers of different molecular weights and shapes (linear, two-arm, four-arm, and eight-arm) were intraductally administered (50 nmol) to female Sprague–Dawley rats. Whole body images were obtained non-invasively. Fluorescence intensities (i.e., amount remaining in duct) were plotted against time to estimate the nanocarrier ductal retention half-lives ($t_{1/2}$). Plasma samples were taken and the pharmacokinetics (Tmax, Cmax) of absorbed nanocarriers was also assessed.

Results The $t_{1/2}$ of linear 12, 20, 30, 40, and two-arm 60 kDa nanocarriers were 6.7 ± 0.9, 16.1 ± 4.1, 16.6 ± 3.4, 21.5 ± 2.7, and 19.5 ± 6.1 h, whereas the four-arm 20, 40, and eight-arm 20 kDa had $t_{1/2}$ of 9.0 ± 0.5, 11.5 ± 1.9, and 12.6 ± 3.0 h. The $t_{1/2}$ of unconjugated fluorescein was significantly lower (14.5 ± 1.4 min). The Tmax for 12, 40, 60 kDa nanocarriers were 1, 24, and 32 h, respectively, and only 30 min for fluorescein.

Conclusions Since normal breast ducts are highly permeable, the use of nanocarriers may be helpful in prolonging ductal retention of diagnostic and/or therapeutic agents.

KEY WORDS ductal carcinoma *in situ* (DCIS) · ductal retention · intraductal drug delivery · non-invasive imaging · PEG nanocarriers

ABBREVIATIONS

Cmax	plasma peak concentration
DCIS	ductal carcinoma *in situ*
DLS	dynamic light scattering
GPC	gel-permeation chromatography
IVIS	*in vivo* imaging system
PEG	poly(ethylene glycol)
PLD	PEGylated liposomal doxorubicin
Tmax	time at which Cmax is reached

INTRODUCTION

DCIS is the proliferation of malignant epithelial cells within the lumen of breast ducts without penetrating the basement membrane (1–3). Each human breast contains 5–9 ductal orifices on the nipple, arranged in central and peripheral groups, that lead to separate and nonanastomosing ductal

Y. Singh and D. Gao contributed equally to this work.

Electronic supplementary material The online version of this article (doi:10.1007/s11095-012-0763-z) contains supplementary material, which is available to authorized users.

Y. Singh · D. Gao · Z. Gu · S. Li · K. A. Rivera · S. Stein · P. J. Sinko (✉)
Department of Pharmaceutics
Ernest Mario School of Pharmacy, Rutgers
The State University of New Jersey
160 Frelinghuysen Road
Piscataway, New Jersey 08854, USA
e-mail: sinko@rci.rutgers.edu

S. Love
Dr. Susan Love Research Foundation
2811 Wilshire Blvd., Suite 500
Santa Monica, California 90403, USA

system, extending to terminal duct lobular units (4). There is an increasing realization that DCIS occurs in one ductal system within the breast (5). DCIS are biologically heterogenous, with variable pathological and clinical features, and are grouped into five architectural subtypes: papillary, micropapillary, cribriform, solid, and comedo (3). It is the comedo form that is associated with higher nuclear grade, aneuploidy, higher proliferation rate, HER2/neu gene amplification/protein over expression, and clinically more aggressive behavior (3). DCIS, even though non-invasive, represents an important stage in the progression to invasive breast cancer (1). The incidence of DCIS has increased significantly over the years. In 1983, only 4800 cases of DCIS were reported in the United States, but now more than 50,000 cases are diagnosed annually (6). It has been estimated that more than one million women in the United States alone will be diagnosed with DCIS by 2020 (7). This increase is attributed to the use of screening mammography, which detects DCIS as microcalcifications and/or soft-tissue densities in the breast.

Even though the exact mechanism of tumorigenesis is not clear, most invasive breast cancers arise from *in situ* carcinomas (1). Therefore, intervention at this stage is expected to prevent the occurrence of invasive breast cancer and provide significant health benefits to women. The main objective of treating DCIS is to prevent local recurrence, in particular of invasive breast cancer (1). Historically, DCIS were treated with mastectomy (excision of the complete breast), which cures 98 % of lesions and is associated with low recurrence (1–2 % of patients). However, the more popular treatment option now is lumpectomy (breast-conserving surgery) in which only the affected areas of the breast are excised. After lumpectomy, women are at varying risk of recurrence of both non-invasive and invasive breast cancer. Most recurrences occur at or near the original site of tumor. Use of radiotherapy further reduces the risk of recurrence, and the estrogen receptor antagonist in breast, tamoxifen, is also used as adjuvant therapy to reduce the likelihood of recurrence in ER positive patients.

Systemic chemotherapy, which is associated with significant systemic toxicities, is not used to treat DCIS since the limited blood supply and location of the cancer within the breast duct makes drug access low and variable. It has been suggested that intraductal access and local treatment (administration of drugs directly into the duct by means of the nipple) may be an effective method of treating DCIS since most breast cancers arise from ductal epithelial cells (1–3) and are located in one ductal system (5). Intraductal therapy provides an opportunity to locally target and treat DCIS (8,9). The development of techniques (e.g., catheters for cannulation, endoscopes, etc.) for accessing the ductal system (10–12) and approaches (nipple aspiratory fluid, ductal lavage, etc.) for analyzing ductal fluids (8,9) make the intraductal approach particularly attractive for local drug delivery. Intraductal therapy is advantageous because it delivers the drug directly to ducts at a concentration not achievable by systemic delivery, and potentially without the toxicities associated with systemic administration, if drug retention in the ducts can be maintained.

McFarlin and Gould, for the first time in 2003, used the intraductal route to infuse retroviral vectors into the mammary gland of rats (13). Later, Okugawa *et al.* showed that intraductally-administered paclitaxel produces significantly reduced tumor burden and total number of mammary carcinoma, compared to intraperitoneally administered paclitaxel in rats with mammary carcinoma (14). In addition, paclitaxel administered through duct did not produce toxic side effects. Sukumar and coworkers investigated the efficacy of intraductally-administered 4-hydroxy tamoxifen and PLD in N-methyl-N-nitrosourea (MNU)-induced rat and HER-2/neu transgenic mouse model (15). Compared to intravenous administration, intraductally-administered PLD caused more effective regression of tumor and prevented tumor development without any systemic toxicity or histopathological changes in mammary glands. Sukumar and coworkers also demonstrated the efficacy of intraductally-administered fluorouracil (5-FU) and carboplatin in same rat model, and later established the feasibility, safety, and maximum tolerated dose of intraductal PLD in a clinical trial in outpatient setting, in women awaiting mastectomy (16). Mahoney *et al.* carried out a preoperative trial in women diagnosed with DCIS to demonstrate the feasibility of using intraductal therapy in community settings (17). Chen *et al.* investigated the difference in plasma concentrations of doxorubicin in female breast cancer patients treated with PLD via intraductal and intravenous route, respectively (18). Love *et al.* recently demonstrated the safety of intraductally-administered PLD and carboplatin in women prior to mastectomy in a phase I clinical trial (19). It is interesting to note that carboplatin ductal permeability appeared to be high in women suggesting that developing ductal retention strategies is warranted.

The objective of this work was to investigate the influence of nanocarrier molecular size and shape on breast duct retention. A low molecular weight diagnostic moiety, fluorescein, was used as a prototypical small molecule agent. Based on the human carboplatin results (19), we hypothesized that most small molecule agents are likely to readily diffuse into the systemic circulation upon intraductal administration. Therefore, drug and diagnostic delivery systems, which can improve local retention in breast ducts, are needed to improve the efficacy of intraductal therapy. Recently, our group has used fluorescein-labeled PEG nanocarriers to assess size-based passive accumulation/targeting including the non-invasive measurement of passive distribution in tumors due to the enhanced permeability and retention (EPR) effect (20). We have used similar approaches to target the liver and lungs (21–23). In

addition, polymeric hydrogels have been designed and developed for ocular drug delivery, and ocular and dermal wound healing applications (24–28). In the current investigation, fluorescein was covalently attached to PEG polymers of varying molecular weight and structure. These fluorescein-labeled PEG nanocarriers were administered into the ducts of female SD rats and retention was measured non-invasively using an optical imaging system (IVIS 100). Plasma samples were taken for three nanocarriers (12, 40, and 60 kDa) and the pharmacokinetics (Tmax, Cmax) of absorbed nanocarriers was also assessed. The studies suggest that both nanocarrier molecular weight and structure influence retention in ducts as well as the elimination rate from the systemic circulation. The present studies will have impact on the future design of polymeric drug delivery systems for intraductal therapy of DCIS.

MATERIALS AND METHODS

Materials

The PEG-amine (linear: 12, 20, 30, and 40; two-arm: 60; and four-arm: 20 and 40 kDa) and PEG-thiol (eight-arm: 20 kDa) polymers were obtained from NOF America (Whitefield, NY). The fluorescein-5-succinimidyl ester and fluorescein-5-maleimide were obtained from Anaspec (San Jose, CA). The N, N-dimethyl formamide (DMF) and ethylene diamine tetraacetate (EDTA) were obtained from Sigma-Aldrich (St. Louis, MO), and Sephadex G 50 (medium) was obtained from Thermo Fisher Scientific (Suwanee, GA). The isoflurane (AErrane) was obtained from Baxter (Deerfield, IL), and Veet was obtained from Reckitt Benckiser North America (Parsippany, NJ). The 0.9 % sodium chloride solution (USP grade) was obtained from Hospira (Lake Forest, IL). The fluorescein-labeled PEG nanocarriers (0.2 ml, 2 mg/ml in water) were analyzed on a Waters Breeze GPC system equipped with refractive index (RI) and ultraviolet (UV) detectors, and a Waters Ultrahydrogel 1000 column (7.8×300 mm). The de-ionized (DI) water was used as the mobile phase (flow rate: 1 ml/min). The molecular weights were estimated on a 4800 Proteomics Analyzer MALDI-TOF/TOF system from Applied Biosystems (ABI). Sinapinic acid (10 mg/ml) dissolved in 50 % aqueous acetonitrile containing 0.3 % trifluoroacetic acid (TFA) was used as matrix. The hydrodynamic radii of polymers were measured by DLS on a Malvern Zetasizer Nano ZS. The non-invasive animal images were obtained on a Xenogen IVIS 100 imaging system from Caliper Life Sciences (Hopkinton, MA), whereas the *ex vivo* fluorescence from plasma was measured using a Genios microplate reader from Tecan (San Jose, CA).

Synthesis and Characterization of Fluorescein-Labeled PEG Nanocarriers

Linear 12, 20, 30, 40; Two-Arm 60; and Four-Arm: 20, 40 kDa

The appropriate PEG-amine polymer (100 mg) was taken in a round bottom flask and dissolved in sodium phosphate buffer (10 ml, 0.1 M, pH, 7.9). The fluorescein-5-succinimidyl ester (5 equiv.) was added to the polymer solution and reaction mixture was stirred in dark at room temperature for 8 h. The product was purified on Sephadex G 50 column using water as eluent. The reaction mixture (10×1.0 ml) was loaded on to the column and high molecular weight fractions were eluted. The column was washed with water to remove the unreacted fluorescein. The high molecular weight fractions were pooled together and lyophilized to obtain pure nanocarriers as yellow flakes, which were characterized by GPC and MALDI-TOF.

Linear 12 kDa. Yield: 79.9 mg; GPC: RT=7.4 (PEG-fluorescein) and 8.9 min (PEG-NH_2); MALDI-TOF (m/z): calculated: 12721.3; observed: 12792.6 Da (PEG-fluorescein).

Linear 20 kDa. Yield: 66.9 mg; GPC: RT=6.7 (PEG-fluorescein) and 8.5 min (PEG-NH_2); MALDI-TOF (m/z): calculated: 21813.3 Da; observed: 22470.8 Da (PEG-fluorescein).

Linear 30 kDa. Yield: 74.3 mg; GPC: RT=6.2 (PEG-fluorescein) and 8.2 min (PEG-NH_2); MALDI-TOF (m/z): calculated: 30753.3 Da; observed: 31323.9 Da (PEG-fluorescein).

Linear 40 kDa. Yield: 72.0 mg; GPC: RT=5.9 (PEG-fluorescein) and 7.9 min (PEG-NH_2); MALDI-TOF (m/z): calculated: 42491.3 Da; observed: 43936.7 Da (PEG-fluorescein).

Two-arm 60 kDa. Yield: 65.8 mg; GPC: RT=5.7 min (PEG-fluorescein) and 7.8 min (PEG-NH_2); MALDI-TOF (m/z): calculated: 58214.3 Da; observed: 58680.2 Da (PEG-fluorescein).

Four-arm 20 kDa**.** Yield: 79.8 mg; GPC: RT=6.1 (PEG-fluorescein) and 8.7 min (PEG-NH_2); MALDI-TOF (m/z): calculated: 20541.3 Da; observed: 22716.7 Da (PEG-fluorescein).

Four-arm 40 kDa. Yield: 70.4 mg; GPC: RT=5.0 (PEG-fluorescein) and 8.1 min (PEG-NH_2); MALDI-TOF (m/z): calculated: 45563.3 Da; observed: 46697.0 Da (PEG-fluorescein).

Eight-Arm 20 kDa

The PEG-thiol polymer (100 mg) was taken in a round bottom flask and dissolved in sodium phosphate buffer (10 ml, 0.1 M, pH, 7.4) containing EDTA (5 mM). The fluorescein-5-maleimide (5 equiv.) dissolved in DMF (0.5 ml) was added to the polymer solution and reaction mixture was stirred in dark at room temperature for 8 h. The crude product was purified on a Sephadex G 50 column as described earlier for 12–60 kDa nanocarriers. The pure nanocarrier was obtained as yellow flakes after freeze-drying, and was characterized by GPC.

Yield: 76.34 mg; GPC: RT=9.6 (PEG-fluorescein) and 9.2 min (PEG-SH).

Hydrodynamic Studies

The hydrodynamic radii of PEG polymers were measured at room temperature using DLS. Polymer solutions (2 mg/ml) were prepared in saline (0.9 % sodium chloride) and passed through a 0.2 μ membrane filter, prior to each measurement. All studies were done in triplicate and data are presented as mean ± SD.

Animals

Female SD rats (6 weeks old) were obtained from Hilltop Lab Animals (Scottdale, PA), and housed in Rutgers Laboratory Animal Services facility accredited by the Association for the Assessment and Accreditation of Laboratory and Care International (AAALAC). The animals were maintained on a 12 h light/dark cycle in a temperature-controlled environment, with food and water *ad libitum*. The animals were acclimatized for at least a day prior to studies, and a protocol approved by the Rutgers University Institutional Animal Care and Use Committee was used for all experiments. A day prior to study, rat body hair was trimmed with a clipper under anesthesia with isoflurane, and skin hair was removed from entire body below the neck using Veet.

Non-Invasive Retention Studies in Breast Ducts

Female SD rats were anesthetized with isoflurane and placed under a surgical microscope. The third nipple (from top) was cleaned with 70 % ethanol. After the dilation of orifice, the nanocarrier solutions in 0.9 % sodium chloride were injected intraductally into the teat (50 nmol) using a 33 G needle attached to a Hamilton syringe (Hamilton, Reno, NV). Fluorescein disodium was used as control. Finally, rats were imaged on an IVIS 100 optical imaging system at different time points. Two untreated rats were used as controls. Following instrument settings were used: Level: High; Em/Ex: GFP; Bin: HR (4); FOV 25; Aperture: f4; and Shutter: 1 s. Fluorescence intensities were plotted against time and $t_{1/2}$ were estimated by non-compartmental pharmacokinetic model using PKSolver (29). The numbers of points for terminal slope were set to auto (default). Each data point represents mean ± SD (n=3).

Mammary Whole Mounts

The nanocarrier solutions in saline were injected into the fourth (from top) teat (50 nmol). At 30 min after injection, rats were euthanized and mammary glands were dissected and fixed in chloroform/isopropanol/acetic acid (6:3:1) for 6 h. The glands were then defatted in toluene for 2 h and stored in biopsy pouches filled with methyl salicylate. Fluorescent images were photographed with Axioskop 2 Plus (Zeiss) using a 2.5 objective lens.

Pharmacokinetic Studies

The fluorescein disodium (control), 12, 40, and 60 kDa nanocarriers were injected into the duct of mammary glands of female SD rats at a dose of 50 nmol in 0.1 ml normal saline. The blood samples (0.1-0.2 ml) were collected from tail vein into the heparin-coated vials at different time points (as indicated in the plots). Plasma was immediately prepared by centrifuging the whole blood for 5 min and collecting the supernatant. The samples were stored at −80°C. Prior to analysis, the plasma samples were thawed and transferred (50 μl) to 96-well plates, and fluorescence was measured on a microplate reader using excitation and emission filters of 485 and 535 nm, respectively. The results were normalized using nanocarrier standard curves in plasma. The maximum concentration (Cmax) and the corresponding sampling time (Tmax) were estimated using a non-compartmental pharmacokinetic model using PKSolver (29). The numbers of point for terminal slope were set to auto (default). Each data point represents mean ± SD (n=3).

Data Analysis

Experimental values were expressed as mean ± standard deviation (SD). The data were analyzed using GraphPad Prism v. 4 software.

RESULTS

Synthesis and Characterization of Fluorescein-Labeled PEG Nanocarriers

In this study, fluorescein was used as a representative low molecular weight diagnostic moiety to investigate the retention of small molecule agents and nanocarriers in normal breast ducts. Fluorescein is a green fluorescent dye with good water solubility, relatively high molar absorptivity, and excellent quantum yield (30). It has been previously used to covalently label peptides, proteins, and oligonucleotides. To obtain fluorescein-labeled PEG nanocarriers of different molecular sizes, PEG polymers of varying molecular weight (12, 20, 30, 40, and 60 kDa) and structure (linear, two-arm, four-arm, and eight-arm), as shown in Fig. 1, were conjugated to fluorescein. In brief, PEG-amines (linear: 12, 20, 30, 40; two-arm 60; and four-arm: 20, 40 kDa) were reacted with fluorescein-5-succinimidyl ester at room

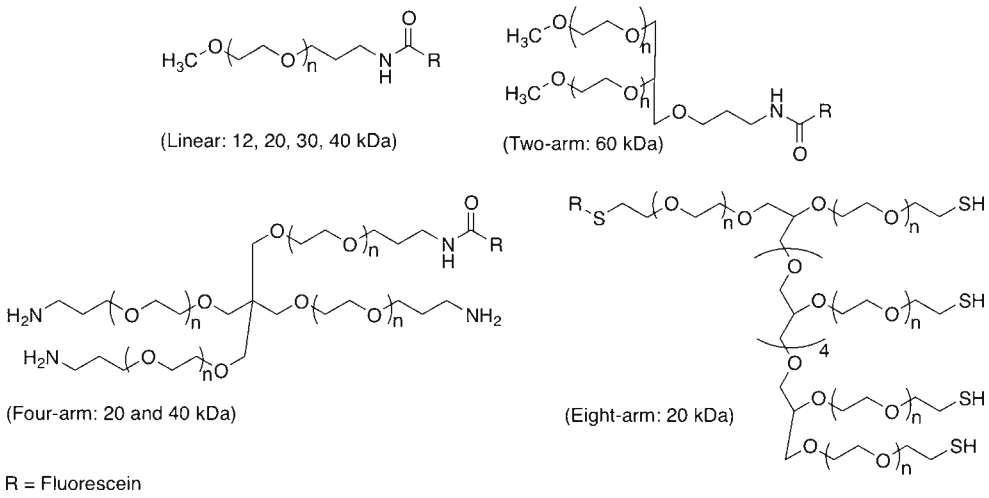

Fig. 1 PEG nanocarriers used for intraductal retention studies in breast ducts. PEG polymers of varying molecular weight (12, 20, 30, 40, and 60 kDa) and structure (linear, two-arm, four-arm, and eight-arm) were conjugated to fluorescein, to investigate the influence of molecular size on ductal retention using a non-invasive optical imaging method.

temperature in sodium phosphate buffer (Scheme 1). Similarly, eight-arm 20 kDa PEG thiol was reacted with fluorescein-5-maleimide at room temperature in sodium phosphate buffer containing EDTA, which was added to maintain the thiol groups in reduced state and to prevent the formation of disulfide bonds. All reactions were carried out in the dark, and nanocarriers were obtained after purification on Sephadex column and subsequent freeze-drying. The yields obtained were in the range of 65–78 %, which indicates efficient coupling. Thus fluorescein was PEGylated using amide or thioether bonds, which are both relatively stable *in vivo* (31).

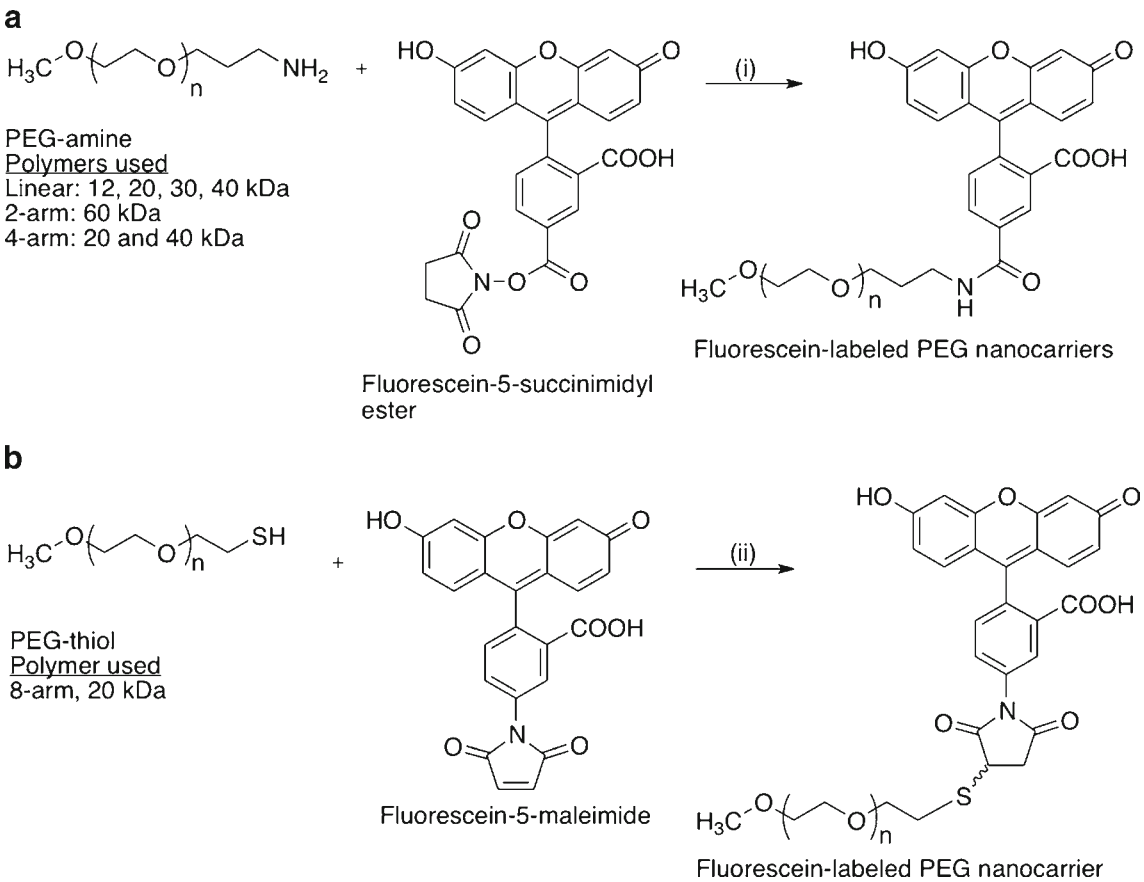

Scheme 1 Synthesis of fluorescein-labeled PEG nanocarriers. The labeled nanocarriers, of different molecular weight and structure, were prepared by reacting PEG-amine and PEG-thiol polymers with fluorescein-5-succinimidyl ester and fluorescein-5-maleimide. Reagents and condition: (i) sodium phosphate buffer (0.1 M, pH, 7.9), room temperature, 8 h; and (ii) sodium phosphate buffer (0.1 M, pH, 7.4) containing EDTA (5 mM), room temperature, 8 h. The nanocarriers were purified using chromatography and characterized by GPC and MALDI-TOF.

The nanocarriers were characterized using a GPC system and MALDI-TOF mass spectrometer (see the Supplementary Material). The retention times, obtained by GPC, for linear 12, 20, 30, 40; two-arm 60; four-arm 20, 40; and eight-arm 20 kDa nanocarriers were founds as 7.4, 6.7, 6.2, 5.9, 5.7, 6.1, 5.1, and 9.6 min, respectively, whereas retention times for corresponding unmodified PEGs were found as 8.9, 8.5, 8.2, 7.9, 7.8, 8.7, 8.1, and 9.2 min, respectively. The retention times for the nanocarriers were lower than the corresponding unmodified PEGs. All nanocarriers were obtained in high purity and no unreacted dye was detected in chromatograms. Furthermore, unmodified PEGs showed peaks at 220 and not 480 nm (absorption max for fluorescein) since PEGs do not absorb at this wavelength, but after conjugation, nanocarriers showed peaks at 220 as well as 480 nm, confirming covalent attachment of fluorescein to PEGs. The molecular weights, estimated by MALDI-TOF, of linear 12, 20, 30, 40; two-arm 60; and four-arm 20, 40 kDa nanocarriers were estimated as 12792.6, 22470.8, 31323.9, 43936.7, 58680.2, 22716.7, and 46697.0 Da, respectively, which were in agreement with their calculated values (see the Materials and Methods section). The eight-arm PEG-fluorescein did not yield satisfactory mass spectrum and was characterized using GPC.

DLS was used to evaluate the influence of polymer molecular weight and structure on the hydrodynamic radii of unmodified PEGs (Table I, also see the Supplementary Material). As the molecular weight increased from 12 to 60 kDa, the hydrodynamic radii increased from 5.416 ± 0.284 to 10.373 ± 0.115 nm. At same molecular weight (e.g., 20 kDa), when the polymer structure was changed from linear to branched (four-arm), the hydrodynamic radii decreased from 7.36 ± 0.199 to 6.827 ± 0.088 nm. Similar trends were observed for linear and four-arm 40 kDa PEGs (9.580 ± 0.354 and 9.251 ± 0.398). However, the hydrodynamic radius of eight-arm 20 kDa PEG was 7.432 ± 0.538 nm, which was higher than linear 20 kDa PEGs. Thus, hydrodynamic radii increased with increase in molecular weight for the linear and branched polymers. For same molecular weight, the hydrodynamic radii decreased with increase in branching in the nanocarrier polymer structure, with the exception of the eight-arm 20 kDa PEG. The odd result obtained for this particular polymer was because of its tendency to aggregate in water, possibly due to intramolecular disulfide bond formation (see the Materials and Methods section). The DLS results were on expected lines, as it has been known that the hydrodynamic radii of linear PEGs increase with increase in molecular weight, and branched PEGs exhibit lower hydrodynamic radii than linear PEGs of similar molecular weight (32).

Table I Hydrodynamic Radii of PEG Polymers Measured using Dynamic Light Scattering

PEG polymers (Mw in kDa)	Hydrodynamic radii in nm (mean ± SD, n=3)
Linear 12	5.416 ± 0.284
Linear 20	7.36 ± 0.199
Linear 30	8.618 ± 0.273
Linear 40	9.580 ± 0.354
Two-arm 60	10.373 ± 0.115
Four-arm 20	6.827 ± 0.088
Four-arm 40	9.251 ± 0.398
Eight-arm 20	7.432 ± 0.538

Polymers were dissolved in saline (0.9 % sodium chloride) (2 mg/ml) and passed through 0.2 μ membrane filters

Non-Invasive Retention Studies in Breast Ducts

The breast ductal retention of fluorescein-labeled PEG nanocarriers of varying molecular weight and structure was investigated using an IVIS 100 small animal imaging system. Female SD rats were used for these studies (n=3). Rats have six pairs of nipples and mammary glands along two mammary chains, and each mammary gland possesses a single ductal system, unlike humans, where each breast has 5–9 ductal systems. The fluorescein disodium (control) or nanocarrier solutions were administered intraductally into the rat teats (50 nmol) under anesthesia, and whole body images were obtained at different time points (Fig. 2). As evident from the figure, fluorescein disodium (control) exhibited extremely short retention in ducts, with signals completely diminishing within 2 h. The PEGylated fluoresceins, on the other hand, exhibited higher retention in ducts. Signals were recorded for up to 32 h for linear 12 kDa, 56 h for linear 20 kDa, and 72 h for the remaining nanocarriers. Thus, an increase in molecular size due to PEGylation resulted in longer nanocarrier retention in ducts presumably due in part to hindered diffusion.

To derive quantitative information from IVIS images, fluorescence intensities from the duct were plotted against time (Fig. 3). The retention half-life, $t_{1/2}$, defined as the time required for fluorescence intensity to reach 50 % of its peak value, was estimated from plots by non-compartmental pharmacokinetic model using PKSolver (Table II) (29). The $t_{1/2}$ of free fluorescein was estimated as 14.5 ± 1.4 min, whereas the $t_{1/2}$ of linear 12 kDa nanocarrier was estimated as 6.7 ± 0.9 h, which increased to 21.5 ± 2.7 h for linear 40 kDa nanocarrier. The $t_{1/2}$ of two-arm 60 kDa, estimated as 19.5 ± 6.1 h, was slightly lower than linear 40 kDa. For branched nanocarriers of different molecular weight, $t_{1/2}$ increased with increase in molecular weight. For nanocarriers of the same molecular weight, the $t_{1/2}$ of four-arm 20 and 40 kDa nanocarriers (9.0 ± 0.5 and 11.5 ± 1.9 h) were lower than corresponding linear nanocarriers (16.1 ± 4.1 and 21.5 ± 2.7 h) possibly due to the more compact nature of the branched nanocarriers. The $t_{1/2}$ of eight-arm 20 kDa nanocarrier, estimated as 12.6 ± 3.0 h, was higher than four-arm 20 and 40 kDa nanocarriers, which as explained earlier was due to its aggregation in water,

resulting from intramolecular crosslinking (disulfide bond formation). In summary, the results obtained were in conformity with the hydrodynamic radii data presented in Table I, and pointed to the fact that both polymer molecular weight and structure influences the molecular size and therefore retention in ducts.

Mammary Whole Mount Studies

The mammary glands (duct) treated with nanocarriers, via intraductal administration, were dissected to prepare whole mounts, and fluorescent images were photographed. Two representative images of ducts treated with 12 and 60 kDa nanocarriers are shown in Fig. 4. As can be seen from the figure, whole mounts of untreated duct did not show fluorescence (Fig. 4a and c), whereas strong fluorescence was observed from whole mounts of duct treated with nanocarriers (Fig. 4b and c). The nanocarriers were uniformly distributed throughout the duct, as evident from the visibility of ductal network in these images.

Pharmacokinetic Studies

The plasma sample for three nanocarriers (linear 12, 40, and two-arm 60 kDa) and unmodified fluorescein (control) were taken to assess the pharmacokinetic (Tmax, Cmax) of absorbed nanocarriers. The plots are shown in Fig. 5 and the Tmax and Cmax values are listed in Table III. The Tmax for 12, 40, and 60 kDa nanocarriers were reached in 1 ± 0.0, 24 ± 12.0, and 32 ± 13.8 h, respectively (Fig. 5b, c, and d), but the Tmax for fluorescein disodium (control) was reached in 30 min only (Fig. 5a). Thus, Tmax increased in the order: fluorescein disodium < linear 12 < linear 40 < two-arm 60 kDa, similar to their order of retention in breast ducts. The Cmax for fluorescein, 12, 40, and 60 kDa nanocarriers were 0.32 ± 0.08, 0.17 ± 0.03, 1.43 ± 0.06, and 1.14 ± 0.07 μM, respectively. The Cmax of 40 and 60 kDa nanocarriers were higher than fluorescein and 12 kDa nanocarrier because the plasma levels of fluorescein and 12 kDa nanocarrier decreased with time but not the 40 and 60 kDa nanocarriers, which remained about the same. This is due to the fact that molecular weights of 40 and 60 kDa nanocarrier are close to or above the renal threshold, which for globular proteins is ~40-60 kDa, and therefore they tend to remain in the blood circulation for longer durations.

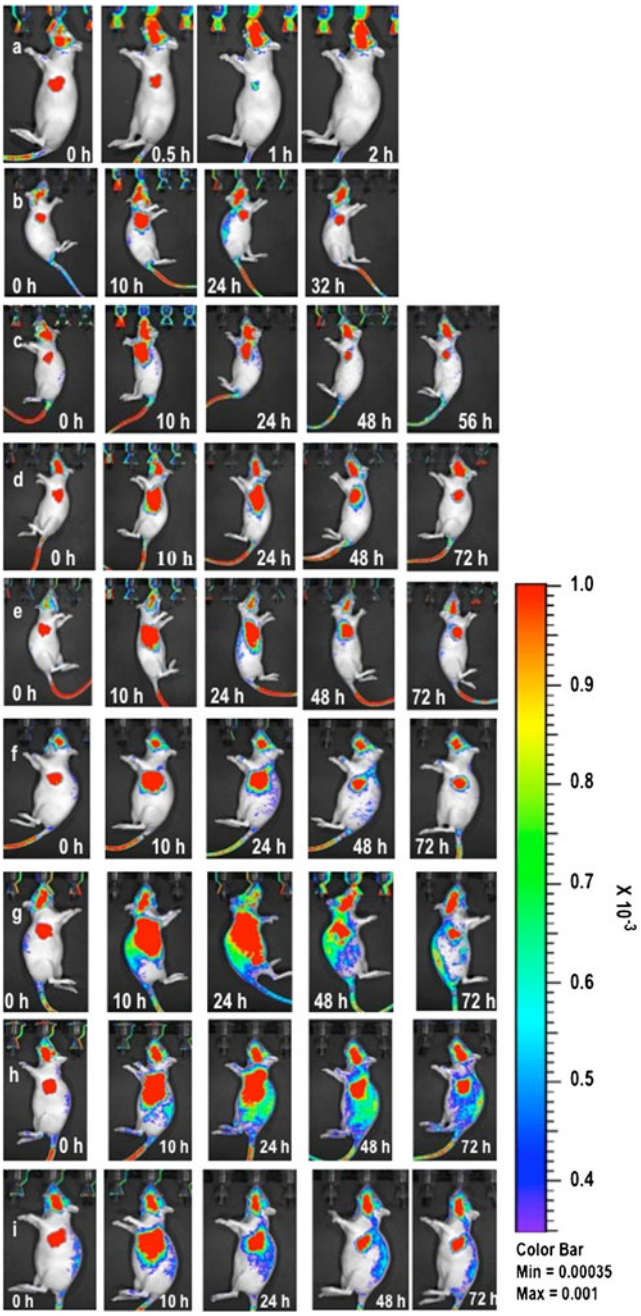

Fig. 2 Intraductal retention of fluorescein-labeled PEG nanocarriers in breast ducts: (**a**) fluorescein disodium (control); (**b**) linear 12 kDa; (**c**) linear 20 kDa; (**d**) linear 30 kDa; (**e**) linear 40 kDa; (**f**) two-arm 60 kDa; (**g**) four-arm 20 kDa; (**h**) four-arm 40 kDa; and (**i**) eight-arm 20 kDa. The solutions for injection were prepared in 0.9 % sodium chloride and administered intraductally into the teat (50 nmol) of female SD rats (n=3), and animals were imaged at different time points on an IVIS 100 system.

DISCUSSION

The interest in intraductal therapy (8,9), which delivers drugs locally to breast ducts, for treating DCIS has risen in recent years because DCIS is located in typically only one of the 5–9 ductal systems present in human breast (5). DCIS remains a local disease for many years and almost all invasive breast cancer arises from these *in situ* carcinomas (1). The obvious advantages are local targeting and a significantly lower risk of systemic drug exposure and the resulting toxicity (14–16,19). A very recent clinical study has firmly

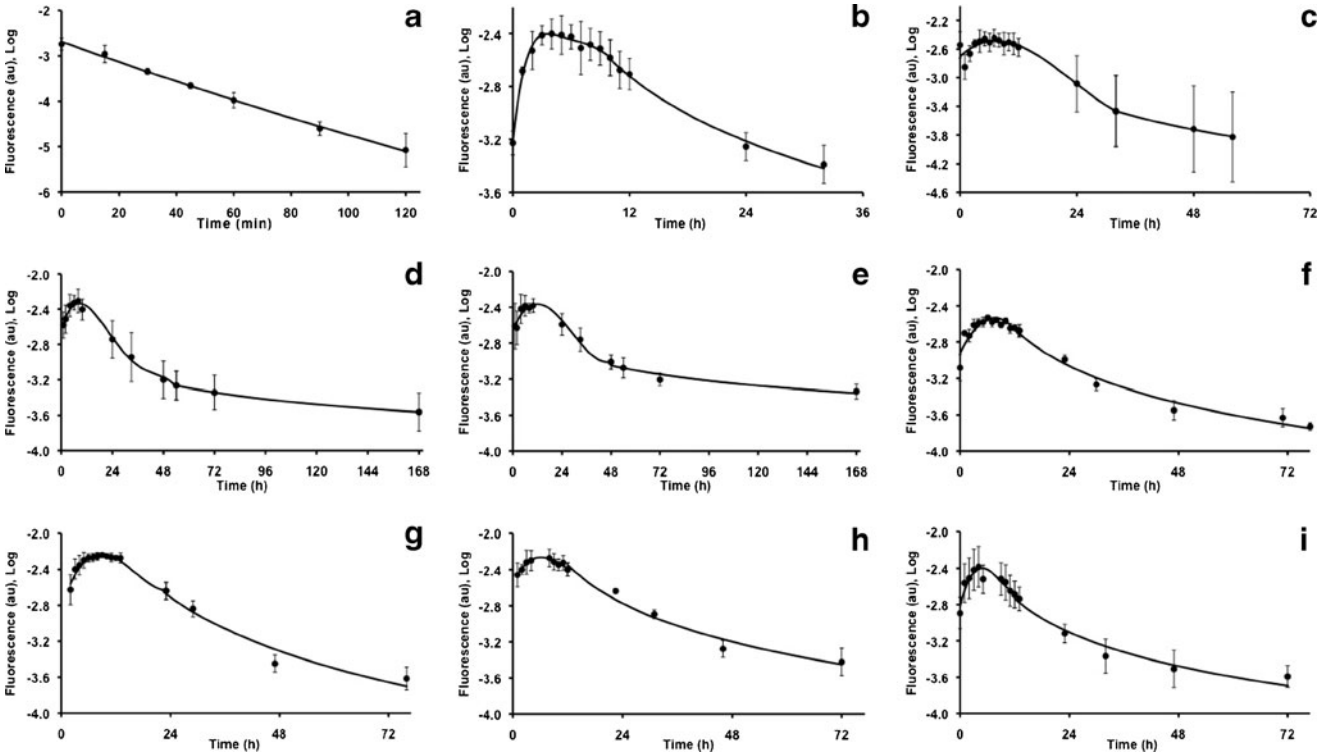

Fig. 3 Nanocarrier distribution in ducts: (**a**) fluorescein disodium (control); (**b**) linear 12 kDa; (**c**) linear 20 kDa; (**d**) linear 30 kDa; (**e**) linear 40 kDa; (**f**) two-arm 60 kDa; (**g**) four-arm 20 kDa; (**h**) four-arm 40 kDa; and (**i**) eight-arm 20 kDa. The $t_{1/2}$ of nanocarriers in duct were estimated from plots by non-compartmental pharmacokinetic model using PKSolver. Each point represents mean ± SD (n=3).

established the feasibility and efficacy of intraductal administration in breast cancer (16). However, questions remain about ductal permeability and the healthy and diseased ductal microenvironment and how these factors may influence the delivery of drugs and imaging agents in diagnosing, treating, and following the progression of DCIS.

Love and coworkers in a phase I study administered carboplatin and PLD by intraductal route to breast cancer patients, prior to mastectomy (19). Pharmacokinetic analysis showed that carboplatin rapidly diffused into the systemic circulation (Tmax: ~30 min), but doxorubicin exhibited delayed peak times (Tmax: >36 h) due to the enhanced retention and sustained release from the liposomal formulation used in the study. Moreover, plasma peak concentrations for intraductal administration were substantially lower than intravenous administration. Similar observations were made in animals. For example, Okugawa *et al.* delivered paclitaxel by the intraductal route to female SD rats bearing MNU-induced mammary carcinoma (14). At a dose of 25 mg/kg, the plasma Cmax for intraductal administration occurred at 6 h, whereas the plasma Cmax for intraperitoneal administration occurred at 3 h. Thus, the Cmax for intraductal administration were considerably lower than intraperitoneal administration most likely due to a formulation effect. Murata *et al.* evaluated the efficacy of intraductally administered PLD in female SD rats bearing MNU-induced mammary carcinoma (15). At a dose of 400 μg (100 μg per duct), doxorubicin levels (10.4 μmol/L) peaked after 24 h, but when the same dose was administered by the intravenous route, drug level (103.7 μmol/L) peaked at 4 h. Taken together, these studies suggest that there is a need to design and develop delivery systems for intraductal therapy that can improve drug retention in ducts (14,15,19).

Table II Half-lives ($t_{1/2}$) of PEG Nanocarriers in Breast Ducts of Rat

PEG nanocarriers (Mw in kDa, 50 nmol/duct)	$t_{1/2}$ (mean ± SD, n=3)
Fluorescein disodium (control)	14.5 ± 1.4 min
Linear 12	6.7 ± 0.9 h
Linear 20	16.1 ± 4.1 h
Linear 30	16.6 ± 3.4 h
Linear 40	21.5 ± 2.7 h
Two-arm 60	19.5 ± 6.1 h
Four-arm 20	9.0 ± 0.5 h
Four-arm 40	11.5 ± 1.9 h
Eight-arm 20	12.6 ± 3.0 h

$t_{1/2}$ is defined as time at which fluorescence reaches 50 % of its peak value

The aim of present studies was to investigate whether nanocarriers of optimal molecular size can be used to improve the retention and local delivery of diagnostic/therapeutic moieties in normal breast ducts. A low molecular weight diagnostic moiety, fluorescein, was selected since, in our pilot

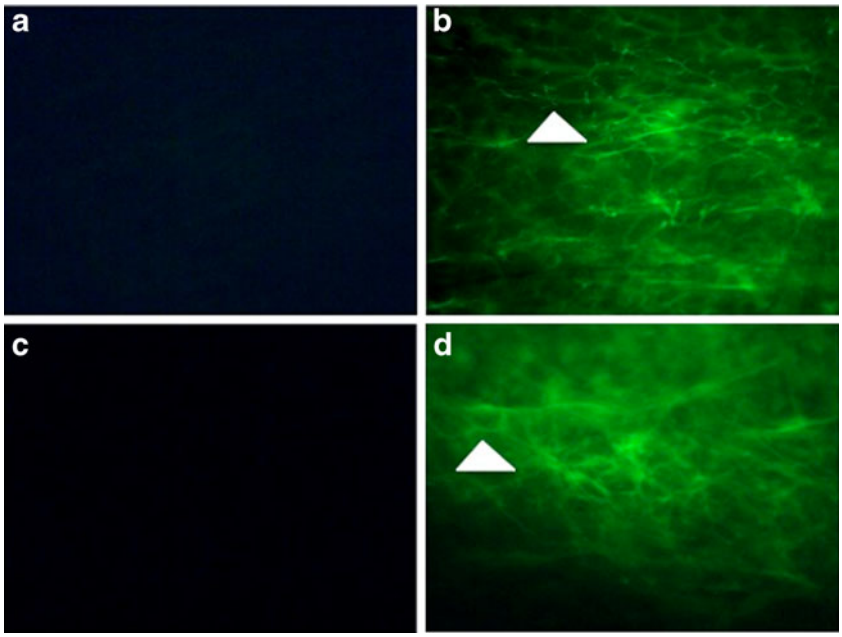

Fig. 4 Mammary whole mounts obtained at 30 min after intraductal administration of nanocarriers: (**a**) untreated duct (contralateral control); (**b**) linear 12 kDa; (**c**) untreated duct (contralateral control); and (**d**) two-arm 60 kDa. *Arrows* indicate ductal network. The ductal network in mammary glands of female SD rat is illuminated due to the intraductal retention of fluorescein-labeled PEG nanocarriers. The images also suggest fairly uniform distribution of nanocarriers through out the ducts.

studies, it was observed to have short ductal retention times. PEG polymers of different molecular weight (12, 20, 30, 40, and 60 kDa) and structure (linear, two-arm, four-arm, and eight-arm) were covalently attached to fluorescein, via relatively stable amide and thioether bonds (31), to vary its molecular size.

PEGs were used as nanocarriers in this work because they are considered a very useful polymer class for clinical

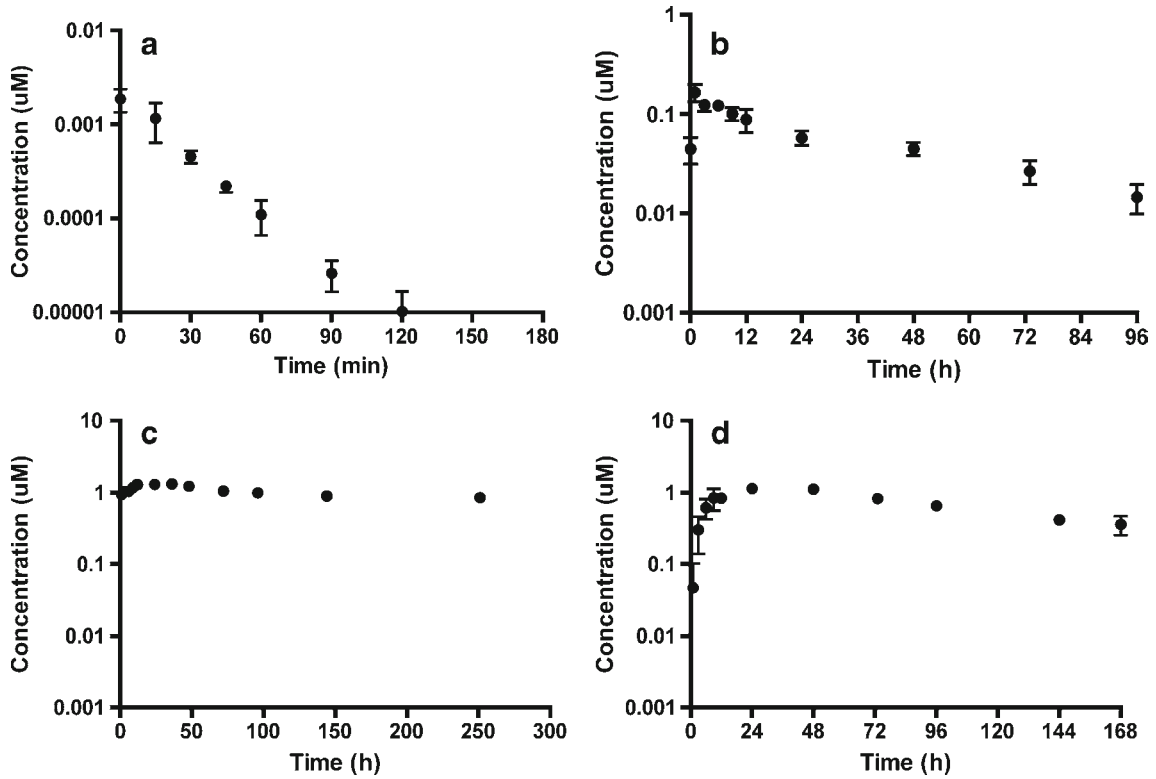

Fig. 5 Pharmacokinetic studies: (**a**) fluorescein disodium (control); (**b**) linear 12 kDa; (**c**) linear 40 kDa; and (**d**) two-arm 60 kDa. The fluorescence from plasma samples were measured on a fluorescence plate reader using excitation and emission filters of 485 and 535 nm, respectively. The results were normalized with nanocarrier standard curve in plasma. The Tmax and Cmax were measured by non-compartmental pharmacokinetic model using PKSolver. Each point represents mean ± SD (n=3).

Table III The Tmax and Cmax of PEG Nanocarriers in Plasma (Mean ± SD, $n=3$)

PEG nanocarriers (Mw in kDa, 50 nmol/duct)	Tmax (h)	Cmax (μM)
Fluorescein disodium (control)	~0.5 ± 0.0	0.32 ± 0.08
Linear 12	1 ± 0.0	0.17 ± 0.03
Linear 40	24 ± 12.0	1.43 ± 0.06
Two-arm 60	32 ± 13.8	1.14 ± 0.07

applications, as they are made of a chemically inert polyether backbone; are nontoxic, non-immunogenic, and non-biodegradable; and show excellent solubility in aqueous media (33–35). Davis and co-workers were the first to demonstrate the use of PEGylation (covalent attachment of PEG) in protein delivery (36,37). Several PEGylated proteins have been approved for clinical use like Adagen (PEG-adenosine deaminase) (38), Oncaspar (PEG-L-asparaginase) (39), Pegasys (40), PEG-Intron (PEG-interferon-α) (41), and krystexxa or pegloticase (PEG-porcine like uricase) (42). The advantage of PEGylation is that PEGylated proteins exhibit increased solubility, greater stability, prolonged plasma half-life, reduced immunogenicity, lower renal clearance, and decreased uptake by cells of reticuloendothelial system (RES) (33). PEGs display large hydrodynamic radii and a coiled/extended conformation and coordinate 2–3 water molecules per ethylene oxide unit when fully hydrated, which increases their apparent molecular weight 5–10 times larger than corresponding globular proteins of comparable mass (43).

The fluorescein-labeled PEG nanocarriers were administered intraductally into the teat of female SD rats, and whole body images were obtained using an IVIS system. The fluorescence intensity obtained from the duct was plotted against time to estimate $t_{1/2}$ of nanocarriers in duct. The $t_{1/2}$ of linear 12, 20, 30, 40, and two-arm 60 kDa nanocarriers were 6.7 ± 0.9, 16.1 ± 4.1, 16.6 ± 3.4, 21.5 ± 2.7, and 19.5 ± 6.1 h, respectively, whereas the $t_{1/2}$ of four-arm 20, 40, and eight-arm 20 kDa nanocarriers were 9.0 ± 0.5, 11.5 ± 1.9, and 12.6 ± 3.0 h, respectively. On the contrary, the $t_{1/2}$ of fluorescein disodium was estimated as only 14.5 ± 1.4 min, consistent with rapid absorption from the duct into the systemic circulation, as expected with a small molecule agent (19). Thus, $t_{1/2}$ increased with increase in molecular weight of linear and branched nanocarriers and, for the same molecular weight nanocarriers, $t_{1/2}$ decreased with an increase in branching in polymer structure. The only notable exception was the eight-arm 20 kDa nanocarrier, which experienced issues with aggregation.

The pharmacokinetics of three nanocarriers (linear 12, 40, and two-arm 60 kDa) and unmodified fluorescein were also assessed. The Tmax for 12, 40, and 60 kDa were reached in 1 ± 0.0, 24 ± 12.0, and 32 ± 13.8 h, respectively, whereas the Tmax for fluorescein disodium was reached in only 30 min. Thus, PEGylation delayed Tmax in a molecular-size dependent manner. The Cmax for fluorescein, 12, 40, and 60 kDa nanocarriers were 0.32 ± 0.08, 0.17 ± 0.03, 1.43 ± 0.06, and 1.14 ± 0.07 μM, respectively. The Cmax of 40 and 60 kDa nanocarriers were higher because their molecular weights are close to or above the renal threshold, which for globular proteins is ~40-60 kDa. Consequently, these nanocarriers remained in blood circulation for a longer duration. The results are expected as Kaminskas *et al.* have shown that PEGylated dendrimers with molecular weight >30 kDa exhibit poor renal clearance and extended elimination half-lives and those with molecular weight <20 kDa are rapidly cleared in urine (44). Even though non-degradable PEGs were used in this study, it is possible to employ degradable polymers in nanocarrier design to ensure their elimination from the body (45).

The above results can be explained using the hydrodynamic data of PEG polymers. The hydrodynamic radii of linear 12, 20, 30, 40, and two-arm 60 kDa polymers were estimated as 5.416 ± 0.284, 7.36 ± 0.199, 8.616 ± 0.273, 9.580 ± 0.354, and 10.373 ± 0.115 nm, respectively. Similarly, the hydrodynamic radii of four-arm 20, 40, and eight-arm 20 kDa polymers were estimated as 6.827 ± 0.088, 9.251 ± 0.398, and 7.432 ± 0.538 nm, respectively. Thus, hydrodynamic radii increased with increase in molecular weight for the linear and branched polymers, and branched polymers exhibited lower hydrodynamic radii than the corresponding linear polymers of same molecular weight, with the exception of eight-arm 20 kDa polymer that showed higher hydrodynamic radii because of aggregation (formation of intramolecular disulfide linkages). It has been previously shown that hydrodynamic radii of linear PEGs increase with increase in molecular weight, and branched PEGs exhibit lower hydrodynamic radii than linear PEGs of similar molecular weight (32).

The present studies are consistent with earlier studies (14,15,19) where fluorescein disodium (control) exhibited an extremely short retention in ducts, similar to carboplatin (19), and it quickly diffused into the systemic circulation. The fluorescein-labeled PEG nanocarriers exhibited enhanced retention in normal rat breast ducts and delayed absorptive clearance similar in pattern to doxorubicin from liposomes (PLD), as suggested by longer Tmax in comparison to fluorescein disodium (15,19). The present studies provide first definitive proof of the fact that nanocarrier molecular size influences the retention of diagnostic and/or therapeutic moieties in normal breast ducts. Understanding the permeability characteristics in normal breast ducts is particularly relevant since (1) DCIS doesn't effect the entire ductal structure and (2) low grade and some moderate grade DCIS cells look and behave very similarly to normal cells. In contrast, high-grade DCIS cells look considerably different than normal cells and are more likely to recur or develop

into an invasive cancer. Currently, we are investigating ductal permeability and its correlation to grade.

In the current studies we limited our investigation to nanocarriers of size ≤10 nm only. Nanoparticles, microparticles, and hydrogels with size ≥10 nm may provide better retention in ducts. Even though not investigated in this work, other physical characteristics (e.g., charge, hydrophilicity/hydrophobicity etc.) may also influence the ductal retention.

CONCLUSIONS

In summary, we have non-invasively assessed the retention of intraductally-administered fluorescein-labeled PEG nanocarriers of varying molecular weights (12, 20, 30, 40, and 60 kDa) and structures (linear, two-arm, four-arm, and eight-arm) in breast ducts of rat. The PEG nanocarriers showed significantly higher retention than fluorescein disodium (control), which exhibited extremely short retention. The estimation of $t_{1/2}$ revealed that retention of nanocarriers in ducts was influenced by both, polymer molecular weight and structure. For both linear and branched nanocarriers, retention in ducts increased with increase in molecular weight, and for nanocarriers of same molecular weight, retention decreased with increase in branching in polymer structure. The only exception was eight-arm nanocarrier, which showed higher retention than corresponding linear and four-arm nanocarriers owing to aggregation. The pharmacokinetic studies revealed that the higher the nanocarrier retention in ducts, the more delayed was the Tmax. Prolonged plasma persistence of the nanocarriers also followed typical size-related effects. This study conclusively proves that using nanocarrier conjugates and altering their molecular size can improve the retention of low molecular weight diagnostic/therapeutic moieties in breast ducts. The data presented here will aid in the design of imaging and drug delivery systems for intraductal diagnostics and therapy to locally target non-invasive cancer in breast ducts.

ACKNOWLEDGMENTS AND DISCLOSURES

This work was supported by grants from Windy Hill Medical, Inc., CA and National Institutes of Health HIT IT program (R01AI084137-01). We also thank Prof. Arash Hatefi at Rutgers University Department of Pharmaceutics for giving us access to Malvern Zetasizer Nano ZS, and Eva Gordon for reading the manuscript.

REFERENCES

1. Burstein HJ, Polyak K, Wong JS, Lester SC, Kaelin CM. Ductal carcinoma *in situ* of the breast. N Engl J Med. 2004;350(14):1430–41.
2. Peterson JL, Vallow LA, Hines SL, Buskirk SJ. Ductal carcinoma *in situ* of the breast. Oncol Rev. 2009;3:237–46.
3. Silverstein MJ. Ductal carcinoma *in situ* of the breast. Annu Rev Med. 2000;51:17–32.
4. Love SM, Barsky SH. Anatomy of the nipple and breast ducts revisited. Cancer. 2004;101(9):1947–57.
5. Holland R, Veling SH, Mravunac M, Hendriks JH. Histologic multifocality of Tis, T1-2 breast carcinomas. Implications for clinical trials of breast-conserving surgery. Cancer. 1985;56(5):979–90.
6. American Cancer Society. Cancer facts and figures 2011. Available from: http://www.cancer.org/Research/CancerFactsFigures/CancerFactsFigures/cancer-facts-figures-2011
7. Virnig BA, Shamliyan T, Tuttle TM, Kane RL, Wilt WJ. Diagnosis and management of ductal carcinoma *in situ* (DCIS): Evidence report/Technology assessment, No. 185. Rockville, MD, 2009
8. Flanagan M, Love S, Hwang ES. Status of intraductal therapy for ductal carcinoma *in situ*. Curr Breast Cancer Rep. 2010;2(2):75–82.
9. King BL, Love SM. The intraductal approach to the breast: raison d'etre. Breast Cancer Res. 2006;8(2):206.
10. Love SM, Barsky SH. Breast-duct endoscopy to study stages of cancerous breast disease. Lancet. 1996;348(9033):997–9.
11. Jacobs VR, Paepke S, Schaaf H, Weber BC, Kiechle-Bahat M. Autofluorescence ductoscopy: a new imaging technique for intraductal breast endoscopy. Clin Breast Cancer. 2007;7(8):619–23.
12. Goulet RJ, Badve S, Brannon-Peppas L, Rouch D, Huntley C, Storniolo AM. Pilot trial assessing the feasibility of intra-ductal delivery of epirubicin (epi)-containing nanoparticles (np) via In-Duct breast microcatheter (IDBM). J Clin Oncol. 2004;22(14S):828.
13. McFarlin DR, Gould MN. Rat mammary carcinogenesis induced by *in situ* expression of constitutive Raf kinase activity is prevented by tethering Raf to the plasma membrane. Carcinogenesis. 2003;24(6):1149–53.
14. Okugawa H, Yamamoto D, Uemura Y, Sakaida N, Tanano A, Tanaka K, Kamiyama Y. Effect of perductal paclitaxel exposure on the development of MNU-induced mammary carcinoma in female S-D rats. Breast Cancer Res Treat. 2005;91(1):29–34.
15. Murata S, Kominsky SL, Vali M, Zhang Z, Garrett-Mayer E, Korz D, Huso D, Baker SD, Barber J, Jaffee E, Reilly RT, Sukumar S. Ductal access for prevention and therapy of mammary tumors. Cancer Res. 2006;66(2):638–45.
16. Stearns V, Mori T, Jacobs LK, Khouri NF, Gabrielson E, Yoshida T, Kominsky SL, Huso DL, Jeter S, Powers P, Tarpinian K, Brown RJ, Lange JR, Rudek MA, Zhang Z, Tsangaris TN, Sukumar S. Preclinical and clinical evaluation of intraductally administered agents in early breast cancer. Sci Transl Med. 2011;3(106):106ra108.
17. Mahoney ME, Mills DJ, Love S. Intraductal therapy of DCIS with liposomal doxorubicin: a preoperative trial in rural California. BMC Proc. 2009;3:S31.
18. Chen Z, Mei D, Dai Y-Y, Tang Z-Q. Plasma concentration of doxorubicin after intraductal administration of doxorubicin long-circulating liposome in patients with breast cancer. Chinese Pharm J. 2010;45(20):1585–8.
19. Love SM, Zhang B, Zhang W, Zhang B, Yang H, Rao J. Local drug delivery to the breast: a phase I study of breast cytotoxic agent administration prior to mastectomy. BMC Proc. 2009;3:S29.
20. Singh Y, Gao D, Gu Z, Li S, Stein S, Sinko PJ. Noninvasive detection of passively targeted poly(ethylene glycol) nanocarriers in tumors. Mol Pharm. 2012;9:144–55.
21. Chao P, Deshmukh M, Kutscher HL, Gao D, Rajan SS, Hu P, Laskin DL, Stein S, Sinko PJ. Pulmonary targeting microparticulate camptothecin delivery system: anticancer evaluation in a rat

orthotopic lung cancer model. Anticancer Drugs. 2010;21(1):65–76.
22. Kutscher HL, Chao P, Deshmukh M, Sundara Rajan S, Singh Y, Hu P, Joseph LB, Stein S, Laskin DL, Sinko PJ. Enhanced passive pulmonary targeting and retention of PEGylated rigid microparticles in rats. Int J Pharm. 2010;402(1–2):64–71.
23. Kutscher HL, Chao P, Deshmukh M, Singh Y, Hu P, Joseph LB, Reimer DC, Stein S, Laskin DL, Sinko PJ. Threshold size for optimal passive pulmonary targeting and retention of rigid microparticles in rats. J Control Release. 2010;143(1):31–7.
24. Anumolu SS, Singh Y, Gao D, Stein S, Sinko PJ. Design and evaluation of novel fast forming pilocarpine-loaded ocular hydrogels for sustained pharmacological response. J Control Release. 2009;137(2):152–9.
25. Anumolu SS, Menjoge AR, Deshmukh M, Gerecke D, Stein S, Laskin J, Sinko PJ. Doxycycline hydrogels with reversible disulfide crosslinks for dermal wound healing of mustard injuries. Biomaterials. 2011;32(4):1204–17.
26. Anumolu SS, DeSantis AS, Menjoge AR, Hahn RA, Beloni JA, Gordon MK, Sinko PJ. Doxycycline loaded poly(ethylene glycol) hydrogels for healing vesicant-induced ocular wounds. Biomaterials. 2010;31(5):964–74.
27. Gordon MK, Desantis A, Deshmukh M, Lacey CJ, Hahn RA, Beloni J, Anumolu SS, Schlager JJ, Gallo MA, Gerecke DR, Heindel ND, Svoboda KK, Babin MC, Sinko PJ. Doxycycline hydrogels as a potential therapy for ocular vesicant injury. J Ocul Pharmacol Ther. 2010;26(5):407–19.
28. Deshmukh M, Singh Y, Gunaseelan S, Gao D, Stein S, Sinko PJ. Biodegradable poly(ethylene glycol) hydrogels based on a self-elimination degradation mechanism. Biomaterials. 2010;31(26):6675–84.
29. Zhang Y, Huo M, Zhou J, Xie S. PKSolver: An add-in program for pharmacokinetic and pharmacodynamic data analysis in Microsoft Excel. Comput Methods Programs Biomed. 2010;99(3):306–14.
30. Haugland RP. Fluorophores and their amine-reactive derivatives. In: Handbook of fluorescent probes and research products. 9 edn. Molecular Probes, Eugene, OR: 2002; pp. 7–78.
31. Singh Y, Spinelli N, Defrancq E. Chemical strategies for oligonucleotide-conjugate synthesis. Curr Org Chem. 2008;12:263–90.
32. Kusterle M, Jevsevar S, Porekar VG. Size of pegylated protein conjugates studied by various methods. Acta Chim Slov. 2008;55(3):594–601.
33. Harris JM, Chess RB. Effect of pegylation on pharmaceuticals. Nat Rev Drug Discov. 2003;2(3):214–21.
34. Veronese FM, Pasut G. PEGylation, successful approach to drug delivery. Drug Discov Today. 2005;10(21):1451–8.
35. Joralemon MJ, McRae S, Emrick T. PEGylated polymers for medicine: from conjugation to self-assembled systems. Chem Commun. 2010;46(9):1377–93.
36. Abuchowski A, van Es T, Palczuk NC, Davis FF. Alteration of immunological properties of bovine serum albumin by covalent attachment of polyethylene glycol. J Biol Chem. 1977;252(11):3578–81.
37. Abuchowski A, McCoy JR, Palczuk NC, van Es T, Davis FF. Effect of covalent attachment of polyethylene glycol on immunogenicity and circulating life of bovine liver catalase. J Biol Chem. 1977;252(11):3582–6.
38. Levy Y, Hershfield MS, Fernandez-Mejia C, Polmar SH, Scudiery D, Berger M, Sorensen RU. Adenosine deaminase deficiency with late onset of recurrent infections: response to treatment with polyethylene glycol-modified adenosine deaminase. J Pediatr. 1988;113(2):312–7.
39. Graham ML. Pegaspargase: a review of clinical studies. Adv Drug Deliv Rev. 2003;55(10):1293–302.
40. Rajender Reddy K, Modi MW, Pedder S. Use of peginterferon alfa-2a (40 KD) (Pegasys) for the treatment of hepatitis C. Adv Drug Deliv Rev. 2002;54(4):571–86.
41. Wang YS, Youngster S, Grace M, Bausch J, Bordens R, Wyss DF. Structural and biological characterization of pegylated recombinant interferon alpha-2b and its therapeutic implications. Adv Drug Deliv Rev. 2002;54(4):547–70.
42. Sundy JS, Becker MA, Baraf HS, Barkhuizen A, Moreland LW, Huang W, Waltrip 2nd RW, Maroli AN, Horowitz Z. Reduction of plasma urate levels following treatment with multiple doses of pegloticase (polyethylene glycol-conjugated uricase) in patients with treatment-failure gout: results of a phase II randomized study. Arthritis Rheum. 2008;58(9):2882–91.
43. Manjula BN, Tsai A, Upadhya R, Perumalsamy K, Smith PK, Malavalli A, Vandegriff K, Winslow RM, Intaglietta M, Prabhakaran M, Friedman JM, Acharya AS. Site-specific PEGylation of hemoglobin at Cys-93(beta): correlation between the colligative properties of the PEGylated protein and the length of the conjugated PEG chain. Bioconjug Chem. 2003;14(2):464–72.
44. Kaminskas LM, Boyd BJ, Karellas P, Krippner GY, Lessene R, Kelly B, Porter CJ. The impact of molecular weight and PEG chain length on the systemic pharmacokinetics of PEGylated poly l-lysine dendrimers. Mol Pharm. 2008;5(3):449–63.
45. Nair LS, Laurencin CT. Polymers as biomaterials for tissue engineering and controlled drug delivery. In: Lee K, Kaplan D, editors. Advances in biochemical engineering/biotechnology, vol. 102. Berlin-Heidelberg: Springer-Verlag; 2006. p. 47–90.